Numerical calculations of the total ac loss of Cu-stabilized $YBa_2Cu_3O_{7-\delta}$ coated conductor with a ferromagnetic substrate

Doan N. Nguyen[a)]
Center for Advanced Power Systems, Florida State University, Tallahassee, Florida 32306 and Department of Physics, Florida State University, Tallahassee, Florida 32306

Pamidi V. P. S. S. Sastry
Center for Advanced Power Systems, Florida State University, Tallahassee, Florida 32310

Justin Schwartz
National High Magnetic Field Laboratory, Florida State University, Tallahassee, Florida 32310; Center for Advanced Power Systems, Florida State University, Tallahassee, Florida 32310; and Department of Mechanical Engineering, FAMU-FSU College of Engineering, Tallahassee, Florida 32310

(Received 2 January 2007; accepted 19 January 2007; published online 6 March 2007)

A numerical model is developed to calculate the total alternating-current (ac) loss of Cu-stabilized $YBa_2Cu_3O_{7-\delta}$ (YBCO) coated conductors with a ferromagnetic substrate when carrying an alternating transport current in an ac background magnetic field. The time evolutions of current and magnetic field distributions along the width of the conductor are calculated by solving the one-dimensional Poisson equation for the magnetic vector potential. In addition to the ac loss dissipated in the superconducting layer, the ferromagnetic loss in the substrate and eddy current loss in the Cu stabilizer are also modeled. In the calculations, the superconducting voltage-current behavior is assumed to follow a power law. The model is capable of addressing other practical aspects of YBCO conductors, including the field dependence of the critical current density, and n value, and nonuniformities in the conductor. The magnetic shielding of the ferromagnetic substrate, however, was ignored in the calculations. Numerical results are compared with analytical and experimental results for some special cases. © *2007 American Institute of Physics*.
[DOI: 10.1063/1.2712180]

I. INTRODUCTION

"Coated conductors" are composed of a biaxially textured $YBa_2Cu_3O_{7-\delta}$ (YBCO) superconductor layer formed on a Ni-alloy substrate with one or more thin buffer layers between them. These conductors have the potential for lower production cost and better electromechanical performance than Bi–Sr–Ca–Cu–O based conductors. With increasing production length, they are becoming the most promising candidate for high temperature superconducting (HTS) devices.[1,2] ac losses, however, are a significant challenge for large-scale power applications and remain one of the most important issues in the development and commercialization of YBCO applications.[3–5]

The coated conductor architecture consists of a substrate (with thickness of 50–100 μm) which is often ferromagnetic, one or more buffer layers, the HTS layer, a thin Ag layer, and a Cu stabilizer layer.[1,6–8] The buffer layers are typically thin insulating oxides and thus neither carry current nor generate heat. The Ag layer is also usually thin ($\sim$5–10 μm) in comparison to the Cu stabilizer (50–100 μm), while the substrate has very high electrical resistivity. Therefore, the eddy current dissipation in the buffer, Ag, and substrate can typically be ignored. If the Ag layer thickness is sufficiently large to be considered in the calculation, an effective stabilizer thickness can be introduced to calculate the eddy current loss for both the Ag and stabilizer layers. Thus, the total conductor ac loss Q_{tt} is the sum of the various loss components from the HTS layer (Q_s), substrate (ferromagnetic loss Q_f), and stabilizer (eddy current loss Q_e),

$$Q_{tt} = Q_s + Q_e + Q_f. \tag{1}$$

Q_s is the sum of transport loss Q_t and magnetization loss Q_m ($Q_s = Q_t + Q_m$) generated in the HTS layer. Understanding the contribution of each loss component to the total loss is an important step for reducing the ac loss of coated conductors.

For an YBCO tape with a HTS layer of thickness d_s and half-width $a \gg d_s$, the conductor can be treated as a thin strip and its ac loss components can be calculated analytically in some specific situations. Assume, for example, that an YBCO tape is placed along the z axis with its cross section in the x-y plane as shown in Fig. 1. The substrate with thickness d_f and Cu stabilizer of thickness d_C are also shown in the figure. The sinusoidal time dependences of the transport current $I(t)$ and applied magnetic field $B(t)$ are assumed as $I(t) = I_0 \sin(2\pi ft)$ and $B(t) = B_0 \sin(2\pi ft + \Delta\varphi)$, respectively. The parameter $\Delta\varphi$ is the phase difference between the transport current and applied magnetic field.

For the situation of only transport current, transport loss in the HTS thin strip was calculated by Norris[9] using conformal mapping transformations and the critical state model,[10]

[a)]Author to whom correspondence should be addressed; electronic mail: nguyen@caps.fsu.edu

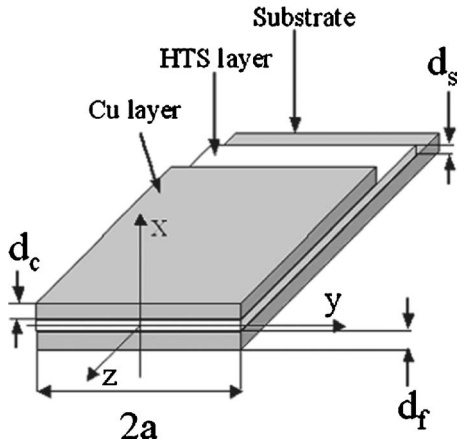

FIG. 1. YBCO conductor with the substrate and stabilizer in *xyz* coordinates (not to scale).

$$Q_t = \frac{\mu_0 I_c^2}{\pi}[(1 - I_0/I_c)\ln(1 - I_0/I_c) + (1 + I_0/I_c)\ln(1 + I_0/I_c) - (I_0/I_c)^2]. \quad (2)$$

In Ref. 11, Müller used Brandt and Indenbom's equations for the current distribution along the width of a thin strip[12] to derive a formula for eddy current loss dissipated in the stabilizer for this case:

$$Q_e = \frac{4\mu_0^2}{\pi^3}\frac{d_C a \omega^2}{\rho} I_c^2 h\left(\frac{I}{I_c}\right), \quad (3)$$

where

$$h(x) = \int_0^x du\sqrt{xu - u^2}\left[1 - \sqrt{1 - u^2} - \frac{u}{2}\ln\frac{1-u}{1+u} + \frac{1}{8}\left(\ln\frac{1+u}{1-u}\right)^2\right]. \quad (4)$$

For the case of perpendicular applied magnetic field only, the magnetization loss, current distribution, and magnetic field distribution of a thin HTS strip were calculated by Brandt and Indenbom.[12] The magnetization loss generated in the HTS layer was derived by integrating the magnetization hysteresis loop and is given by

$$Q_m = 4\mu_0 w_t^2 J_c H_a g\left(\frac{H_a}{H_c}\right), \quad (5)$$

with

$$g(x) = \frac{2}{x}\ln\cosh x - \tanh x. \quad (6)$$

In Eq. (5), $H_c = J_c/\pi$. Based on current and magnetic field distributions calculated by Brandt and Indenbom, Müller estimated the eddy current loss in the stabilizer in this situation as[11]

$$Q_e = \frac{8\mu_0}{3\pi}\frac{d_C a \omega^2}{\rho} H_0^2 h\left(\frac{H_0}{H_c}\right), \quad (7)$$

$$h(x) = \int_0^x du\sqrt{xu - u^2}\left(1 - \frac{3}{\cosh^2 u} + \frac{2}{\cosh^3 u}\right). \quad (8)$$

In previously published work, analytical calculations of Q_s with simultaneous transport current and applied magnetic field are only available when the current and the magnetic field are in phase ($\Delta\varphi = 0$).[12–14] As reported by Schönborg,[14] Q_s was calculated by two equations, one for the low current, high-field regime and the other for the high current, low-field regime. There is no analytical model for calculating eddy current loss in the stabilizer in the case of simultaneous transport current and applied magnetic field.

It is also worth noting that the above analytical calculations for ac losses in HTS strips are based on the critical state model. In addition, those calculations only apply for field-independent critical current and *n* value and a laterally uniform J_c distribution. The analytical calculations, therefore, cannot give a complete description of ac losses in a real conductor. In this paper, numerical calculations of all the ac loss components for an YBCO coated conductor are reported. The numerical calculations are capable of taking into account important, realistic parameters such as field-dependent J_c and *n* value, lateral dependence of J_c, and a phase difference between the transport current and magnetic field. All values of transport current and applied magnetic field referred to in this paper should be understood as their amplitudes.

II. NUMERICAL CALCULATIONS

A. ac loss in HTS layer

The critical state model idealizes the conductor electromagnetic behavior by assuming that the local current density is either equal to the critical current density J_c or is identically zero. In fact, the *V-I* characteristics of real HTS conductors are better described by a power law:[15]

$$E = E_c \frac{\mathbf{J}_z}{j_z}\left[\frac{J_z}{J_c(B)}\right]^{n(B)}, \quad (9)$$

where E_c is the critical electric field criterion used to determine the critical current. E_c is conventionally chosen to be 1 or 0.1 μV/cm. Equation (9) will be used here.

The numerical analysis is based on Brandt's model,[16] solving Maxwell's equations in integral form for the cross section of the superconducting tape. If the perpendicular applied field is in the *x-y* plane, $B_a = (B_x, 0, 0)$ as seen in Fig. 1, then the general equation for the time evolution of the current density distribution is[16–18]

$$E_c \frac{\mathbf{J}_z}{J_z}\left[\frac{J_z(\mathbf{r},t)}{J_c(B)}\right]^{n(B)} + \nabla_z\varphi(t) - y\dot{B}_x(t) = \mu_0\int_s d^2\mathbf{r}' Q(\mathbf{r},\mathbf{r}')\dot{J}_z(\mathbf{r}',t), \quad (10)$$

where $\mathbf{r} = (x, y)$, $\mathbf{r}' = (x', y')$, $\nabla_z\varphi$ is the scalar potential gradient along the *z* axis and is a constant over the tape cross section, *S* is the conductor cross-sectional area, and the kernel $Q(\mathbf{r},\mathbf{r}')$ is defined as[16]

$$Q(\mathbf{r},\mathbf{r}') = \frac{\ln(|\mathbf{r}-\mathbf{r}'|)}{2\pi}. \tag{11}$$

Integrating the current density distribution over the conductor cross section gives the transport current flowing in the wire,

$$I(t) = I_0 \sin(2\pi f t) = \int_S J_z(\mathbf{r},t)d^2r. \tag{12}$$

For YBCO conductor with thickness d and half-width $a \gg d$, the conductor can be treated as a one-dimensional thin film with the sheet critical current density $J_c(y)$. In this limit, Eqs. (10) and (12) transform to

$$E_c \frac{\mathbf{J}_z}{J_z}\left[\frac{J_z(y,t)}{J_c(B)}\right]^{n(B)} + \nabla_z\varphi(t) - y\dot{B}_x(t) = \mu_0 \int_{-a}^{a} du Q(y,u)\dot{J}_z(u,t), \tag{13}$$

$$I(t) = I_0 \sin(2\pi f t) = \int_{-a}^{a} J_z(y,t)dy. \tag{14}$$

Equations (13) and (14) can be solved numerically by transforming them into discrete forms. In Eq. (13), however, the kernel $Q(y,u)=\ln|y-u|/2\pi$ has a logarithmic singularity at $y=u$. This problem is overcome by substituting for y and u an odd function $y=y(s)=u(s)$ using a new variable s. This odd function must satisfy $u(0)=0$ and $u(1)=a$, and its derivative, $u'(s)=v(s)$, vanishes at $s=1$, i.e., $v(1)=0$. For instance, two such functions[19,20] are

$$u(s) = a\left(\frac{3}{2}s - \frac{1}{2}s^3\right) \text{ and } u'(s) = \frac{3}{2}a(1-s^2) = v(s), \tag{15}$$

$$u(s) = a\left(\frac{15}{8}s - \frac{5}{4}s^3 + \frac{15}{8}s^5\right) \text{ and } u'(s) = \frac{3}{2}a(1-s^2)^2 = v(s). \tag{16}$$

To transform Eqs. (13) and (14) into discrete forms, variable s is discretized into $2N$ equidistant points, $s_i=(i-1/2)/N-1$, with $i=1,2,\ldots,2N$. With the variable substitution,

$$\int_{-a}^{a} dy = \int_{-1}^{1} v(s)ds = \sum_{i=1}^{2N} v(s_i)/N = \sum_{i=1}^{2N} w_i, \tag{17}$$

where $w_i=v(s_i)/N$. Equations (13) and (14) then become

$$E_c \frac{\mathbf{J}_i}{J_i}\left[\frac{J_i(t)}{J_c(B)}\right]^{n(B)} + \nabla_z\varphi - y_i\dot{B}_i(t) = \mu_0 \sum_{j=1}^{2N} Q_{ij}\dot{J}_j(t) \tag{18}$$

and

$$I(t) = \sum_{i=1}^{2N} J_i w_i, \tag{19}$$

with $y_i=y(v_i)$, $J_i(t)=J(y_i,t)$, $\dot{B}_i(t)=\dot{B}(y_i,t)$, and $Q_{ij}=Q(y_i,y_j)w_j$.

Returning to the problem of the divergence of Q_{ij} when $i=j$, with the variable substitution $y=y(s)$ as shown above, $v(s)\neq 0$ for $0<s<1$. Thus, the difference $|y_i-y_j|$ is replaced by $v_i/2\pi N$ when $i=j$. The complete definition of the kernel matrix is therefore given by

$$Q_{ij} = \frac{w_i}{2\pi}\ln|y_i - y_j| \quad \text{for } i \neq j, \tag{20}$$

$$Q_{ij} = \frac{w_i}{2\pi}\ln\frac{w_i}{2\pi} \quad \text{for } i = j. \tag{21}$$

Using the inverse matrix Q_{ij}^{-1} of Q_{ij}, Eq. (18) is rewritten as

$$\dot{J}_i(t) = \frac{J_i(t+\Delta t) - J_i(t)}{\Delta t} = \frac{1}{\mu_0}\sum_{j=1}^{2N} Q_{ij}^{-1}\left\{E_c\frac{\mathbf{J}_j}{J_j}\left[\frac{J_j(t)}{J_c(B)}\right]^{n(B)} + \nabla_z\varphi - y_j\dot{B}_j(t)\right\}. \tag{22}$$

Integrating Eq. (22) over the width of the conductor, we get

$$I(t+\Delta t) = I(t) + \frac{\Delta t}{\mu_0}\sum_{i=1}^{2N} w_i \sum_{j=1}^{2N} Q_{ij}^{-1}\left\{E_c\frac{\mathbf{J}_j}{J_j}\left[\frac{J_j(t)}{J_c(B)}\right]^{n(B)} + \nabla_z\varphi - y_j\dot{B}_j(t)\right\}. \tag{23}$$

With the boundary condition that $J(0)=0$, the scalar gradient $\nabla_z\varphi$ is calculated from Eq. (23). From the known $\nabla_z\varphi$ and Eq. (22), the current distribution along the width of the conductor is calculated. To reduce the computing time, arrays w_i and Q_{ij} are calculated only once at the beginning of the calculation. From the calculated current distribution, the total ac loss and the transport loss of the superconducting layer per unit length, per cycle, are given by

$$Q_s = Q_m + Q_t = \int_{1/f}\int_{-a}^{a} E_z J_z(y)dydt = \int_{1/f}\int_{-a}^{a} E_c\frac{\mathbf{J}_z}{J_z}\left[\frac{J_z}{J_c(B)}\right]^{n(B)} J_z dydt \tag{24}$$

and

$$Q_t = -\int_{1/f}\int_{-a}^{a} \nabla_z\varphi J_z dydt. \tag{25}$$

In the calculation, self-field should be taken into account and thus the perpendicular magnetic field along the width of the conductor is the superposition of the applied field and self-field:

$$B_{x,i}(t) = B_x(t) + \sum_{j=1}^{N} Y_{ij}J_j(t), \quad Y_{ij} = \frac{\mu_0 w_j}{2\pi(y_i - y_j)} \quad \text{for } i \neq j \text{ and } Y_{ij} = 0 \quad \text{for } i = j. \tag{26}$$

The time evolutions of the magnetic field distribution are used to calculate the field dependence of the n value and critical current density. It is also used to compute the eddy current loss and ferromagnetic loss.

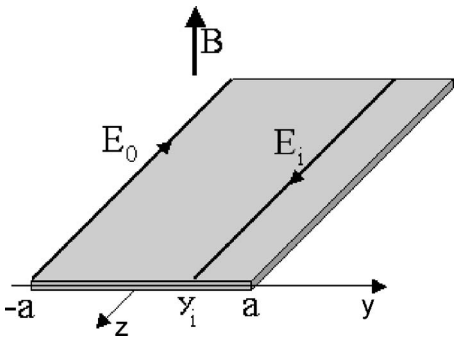

FIG. 2. An imagined loop on the stabilizer formed by the negative edge and a line at y_i position (not to scale).

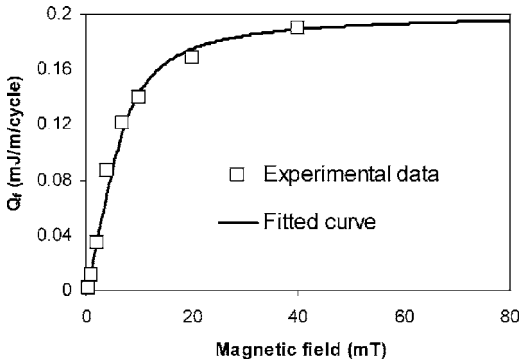

FIG. 3. Dependence of ferromagnetic loss in the substrate on perpendicular magnetic field (Refs. 23 and 24).

B. Eddy current loss

The eddy current power loss per unit length in the stabilizer at time t is calculated using

$$Q_e(t) = \int_{S_C} E_e(x,y,t) J_e(x,y,t) dxdy, \tag{27}$$

where S_C is the cross-sectional area of the Cu stabilizer. The electric field $E_e(x,y,t)$ and eddy current density $J_e(x,y,t)$ obey Ohm's law,

$$E_e(x,y,t) = \rho_C J_e(x,y,t), \tag{28}$$

where ρ_C is the Cu resistivity.

Since $a \gg d_S$ and $a \gg d_C$, both the superconductor and stabilizer layers are considered as thin films and therefore one can ignore the x dependence of the eddy current density and electric field along the thickness of the stabilizer. Using Eqs. (17) and (28) and assuming that the sample is long enough to ignore end effects, the integral in Eq. (27) becomes the discrete form

$$Q_e(t) = \sum_{i=1}^{2N} \frac{E_i^2(t)}{\rho_C} w_i d_C, \tag{29}$$

where $E_i = E_e(y_i)$. Faraday's law is applied for a unit length of a loop formed between the negative edge of the stabilizer at $y=-a$ and a line at position y_i as shown in Fig. 2,

$$E_i - E_0 = \frac{\partial \phi_i(t)}{dt}. \tag{30}$$

In this equation, magnetic flux $\phi_i(t)$ is defined as

$$\phi_i(t) = \mu_0 \int_{-a}^{y_i} H(y,t) dy = \mu_0 \sum_{j=1}^{i} H(y_j,t) w_j = \mu_0 \sum_{j=1}^{i} H_j(t) w_j. \tag{31}$$

Thus, Eq. (30) becomes

$$E_i = E_0 + \mu_0 \frac{\partial}{\partial t} \sum_{j=1}^{i} H_j(t) w_j. \tag{32}$$

Using charge conservation, the total eddy current along the z axis in the stabilizer must be zero. Therefore,

$$0 = \sum_{i=1}^{2N} j_i w_i d_C = \sum_{i=1}^{2N} \frac{E_i}{\rho_C} w_i d_C = \sum_{i=1}^{2N} \frac{w_i d_C}{\rho_C} \left[E_0 + \mu_0 \frac{\partial}{\partial t} \sum_{j=1}^{i} H_j(t) w_j \right] \tag{33}$$

or

$$E_0 = -\mu_0 \sum_{i=1}^{2N} w_i \frac{\partial}{\partial t} \sum_{j=1}^{i} H_j(t) w_j \Big/ \sum_{i=1}^{2N} w_i. \tag{34}$$

For each time step, the magnetic field distribution is calculated using Eq. (26). Using that calculation with Eq. (34), E_0 is determined and then substituted into Eq. (32) to calculate E_i. The eddy current loss in the stabilizer is then determined by Eq. (29).

If the Ag layer is not very thin (for instance, the Ag layer thickness is greater than 10% of the Cu stabilizer thickness), the eddy current loss generated in this layer must also be considered. In this case, the total eddy current losses in both Cu and Ag layers are calculated using an effective thickness d_{eff}, which replaces d_C in Eq. (29):

$$Q_e(t) = \sum_{i=1}^{2N} \frac{E_i^2(t)}{\rho_C} w_i d_{\text{eff}}. \tag{35}$$

The effective thickness d_{eff} is calculated by

$$d_{\text{eff}} = \frac{d_C \rho_A + d_A \rho_C}{\rho_A}, \tag{36}$$

where ρ_A and d_A are the resistivity and thickness of the Ag layer, respectively.

C. Ferromagnetic loss in the substrate

Recent publications show that the ferromagnetic loss can be significant, particularly when only a transport current is present.[21–23] The dependence of ferromagnetic loss on applied magnetic field is measured from magnetization hysteresis of a HTS tape in a superconducting quantum interference device (SQUID) magnetometer at $T > T_c$. For example, the dependence of ferromagnetic loss on applied field amplitude for a Ni5%W substrate with dimensions of 1 cm width and 75 μm thickness is shown in Fig. 3.[23,24] Based on clas-

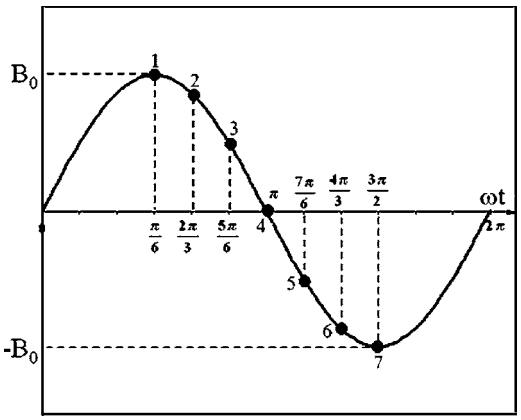

FIG. 4. One full cycle of magnetic field, illustrating the seven times at which calculations are made.

sical theory for magnetization, the data in Fig. 3 are fitted with the function[25]

$$Q_f(B) = C\left[\coth(kB) - \frac{1}{kB}\right], \tag{37}$$

where C and k are constants and B is the applied magnetic field. To get a better fit, however, the B dependence of k may be taken into account. Thus, $Q_f(B)=C[\coth(kB)^m - 1/(kB)^m]$ is chosen to fit the experimental data in Fig. 3. With B in millitesla and Q_f in mJ/m cycle, the fitting curve becomes

$$Q_f(B) = 2\left[\coth(0.28B)^{1.2} - \frac{1}{(0.28B)^{1.2}}\right], \tag{38}$$

which is also plotted in Fig. 3. It is worth noting that the ferromagnetic loss is frequency independent and nearly temperature independent in the range of 50–100 K.[24] The magnetic field amplitude at position y_i is generally determined as the maximum field at that position in a cycle and it is calculated using Eq. (26). In the case of either transport current or magnetic field only, the magnetic field amplitude at each point y_i is found at the time when the peak transport current or applied magnetic field occurs. Otherwise, the magnetic field at any point is compared for all the time steps in a half-cycle to determine the magnetic field amplitude at that point. When the distribution of the magnetic field amplitude along the width of the conductor is known, Eq. (38) is used to calculate the ferromagnetic loss.

III. RESULTS AND DISCUSSION

To prevent error due to effects related to the initial conditions as reported in Ref. 18, the first half-period was ignored in the calculation and all the calculated results were obtained in the second half-cycle and thereafter.

The numerical calculations can account for many practical aspects of the conductor, including the lateral dependence of critical current density, magnetic field dependence of critical current and n value, and a phase difference between the transport current and applied magnetic field. To compare with analytical models, the results reported here are for the special case in which $\Delta\varphi=0$, J_c is field independent and uniform, and n value is field independent. The analytical, numerical, and experimental results presented in this paper were obtained for an YBCO coated conductor with a 75 μm thick NiW substrate, a thin YBCO layer, and a 75 μm thick Cu stabilizer. The critical current and n value at 77 K are 186 A and 22, respectively. The results are presented for three specific situations: (A) magnetic field applied perpendicular to the tape without transport current, (B) transport current is passed through the tape without a background magnetic field, and (C) both a perpendicular magnetic field and a transport current are applied.

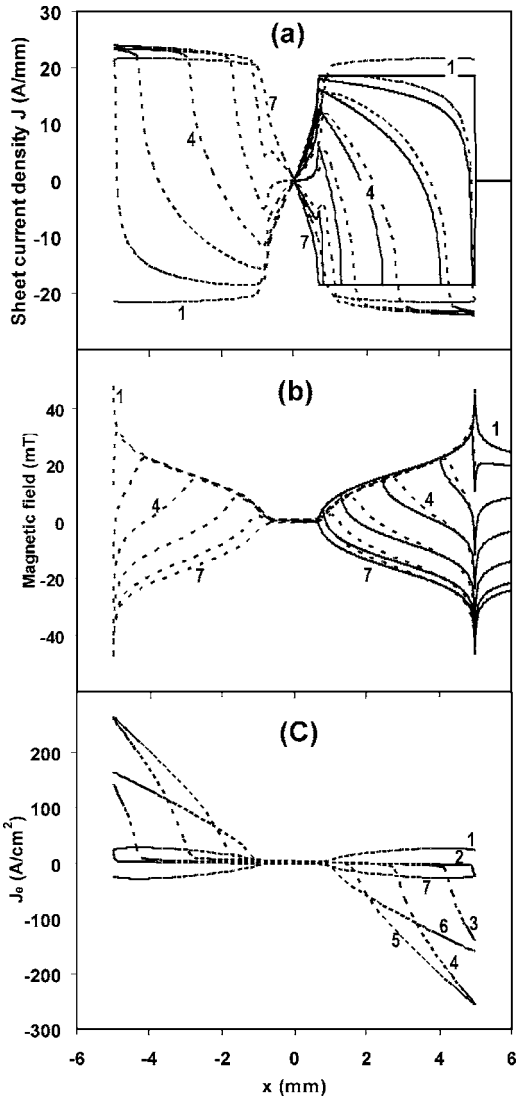

FIG. 5. (a) Current density $J(y)$, (b) magnetic field $B(y)$, and (c) eddy current density $J_e(y)$ are plotted for the seven times indicated in Fig. 4. In (a) and (b), analytical results (solid lines) are plotted for the positive half of the conductor and numerical result (dashed lines) are plotted everywhere. (c) shows only numerical results.

A. Conductor in perpendicular magnetic field

Consider the case of an ac magnetic field, $B(t)$, applied perpendicular to the wide surface of the conductor. To determine the current and magnetic field distributions versus time, consider seven moments in time during a half-cycle such that $B(t)$ decreases from $B_0=20$ mT to $-B_0=-20$ mT. The seven "snapshots" in time are illustrated in Fig. 4. Figures 5(a) and

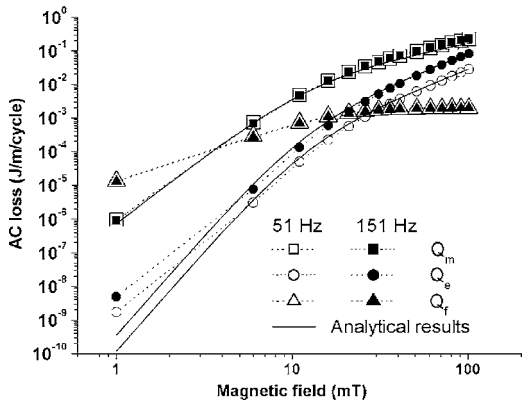

FIG. 6. Numerical results of Q_m, Q_f, and Q_e for frequencies of 51 Hz (dotted lines with open symbols) and 151 Hz (dotted lines with filled symbols). Corresponding analytical results (solid lines) are also plotted.

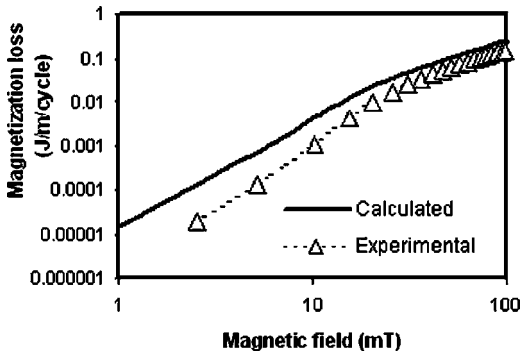

FIG. 7. Total magnetization loss as a function of magnetic field determined numerically (solid line) and experimentally (symbol).

5(b) show the current distribution $J(y)$ and magnetic field $B(y)$ corresponding to these seven times as calculated from both the numerical model (dashed lines) and the analytical equations given by Brandt and Indenbom in Ref. (solid lines). The analytical results are plotted only in the positive half of the conductor for clarity of the figure. The numerically calculated $J(y)$ and $B(y)$ with a power law ($n=22$) are in general agreement with those calculated by Brandt and Indenbom using the critical state model. Figure 5(c) shows the distribution of the eddy current density $J_e(y)$ calculated numerically over the stabilizer width. The eddy current density is asymmetric with respect to the z axis because of the symmetry of the magnetic field distribution as shown in Fig. 5(b). For the charge conservation, the eddy currents must form closed loops. In this case, the eddy current loops are formed between two regions near the edges of the stabilizer. The eddy currents run along one edge, cross the stabilizer, and then run along the other edge in the opposite direction. Therefore, when $B(t)$ changes from B_0 to $-B_0$, the eddy current density is higher near the edges of the tape and becomes zero at a certain distance from the center of the stabilizer. The zero eddy current portions near the tape center correspond to the nonvarying portions of $B(y)$ in Fig. 5(b).

The ac loss components Q_m, Q_f, and Q_e calculated numerically for applied magnetic field ranging from 1 to 100 mT at frequencies of 51 and 151 Hz are plotted in Fig. 6. The open symbols correspond to the results at 51 Hz and the filled symbols are results at 151 Hz. The magnetization loss in the HTS layer, Q_m, and the ferromagnetic loss Q_f are frequency independent as expected. The eddy current loss component in the Cu layer, Q_e, increases by a factor of 2–4 as the frequency changes from 51 to 151 Hz. Overall, Q_m is the dominant ac loss component. Ferromagnetic loss Q_f plays an important role only in the low-field ($B_0 < 5$ mT) region and becomes less than Q_e for $B_0 > 20$ mT. The eddy current loss changes rapidly with increasing field and frequency and becomes significant at 151 Hz. Analytical results for Q_m calculated from Eq. (5) and for Q_e calculated from Eq. (7) are also plotted in Fig. 6 for comparison. Good agreement between numerical and analytical results is observed for magnetization loss. There is a small variation between the calculations of eddy current loss at low magnetic field. This suggests that the n value affects Q_e more significantly than Q_m. Figure 7 plots numerical and experimental results for the total magnetization loss in the sample, $Q_{\mathrm{mag}} = Q_s + Q_e + Q_f$, for applied magnetic field ranging from 1 to 100 mT. There are differences between the calculated and experimental results, especially at low magnetic field. The numerical calculation needs to be improved by considering nonidealized conductor properties. In addition, the ferromagnetic layer may shield some external field from the HTS layer; this shielding effect is neglected in the numerical calculations. In the calculations, the current distribution on the HTS layer is computed only from the uniform applied field.

B. Conductor with a transport current

Now consider the situation where there is only transport current $I(t)$ in the conductor and no applied magnetic field. The current distribution $J(y)$ and magnetic field $B(y)$ for $I_0 = 167.4$ A $(0.9I_c)$ are plotted in Figs. 8(a) and 8(b) for the same seven times shown in Fig. 4. Again, good agreement between numerical (dashed lines) and analytical (solid lines) results is observed. $B(y)$ calculated analytically using Brandt and Indenbon's equation[12] penetrates the conductor slightly further than the computational result. Unlike the previous case, the eddy current density $J_e(y)$ shown in Fig. 8(c) is symmetric with respect to the z axis as a result of the asymmetric magnetic field distribution shown in Fig. 8(b). In this case, the separate eddy current loops are formed between either edge of the stabilizer and its center. Therefore, $J_e(y)$ near the center of the sample is a nonzero constant, corresponding to the "frozenlike" portions of $B(y)$ observed in Fig. 8(b).

The ac losses for this case are shown in Fig. 9. The transport loss and the eddy current loss calculated analytically from Eqs. (2) and (3) are plotted. There is good agreement between the numerical and analytical results for Q_t while some differences are observed for Q_e, especially for the low and high current regions. The difference between numerical and analytical calculations of Q_e is explained by two factors. The first is the difference in the assumed n value; the second is from an assumption in Müller's calculation[11] that the eddy current electric field in the center of the stabilizer is zero. In fact, as seen in Fig. 8(c), E_e is a nonzero constant near the tape center.

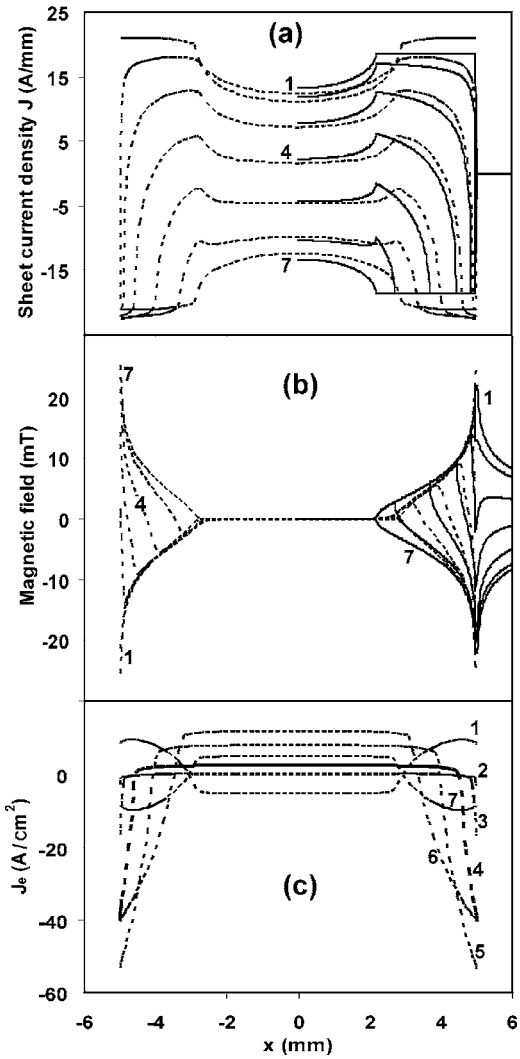

FIG. 8. (a) Current density $J(y)$, (b) magnetic field $B(y)$, and (c) eddy current density $J_e(y)$ are plotted for the seven times indicated in Fig. 4. In (a) and (b), analytical results (solid lines) and numerical results (dashed lines) are shown. (c) shows only numerical results.

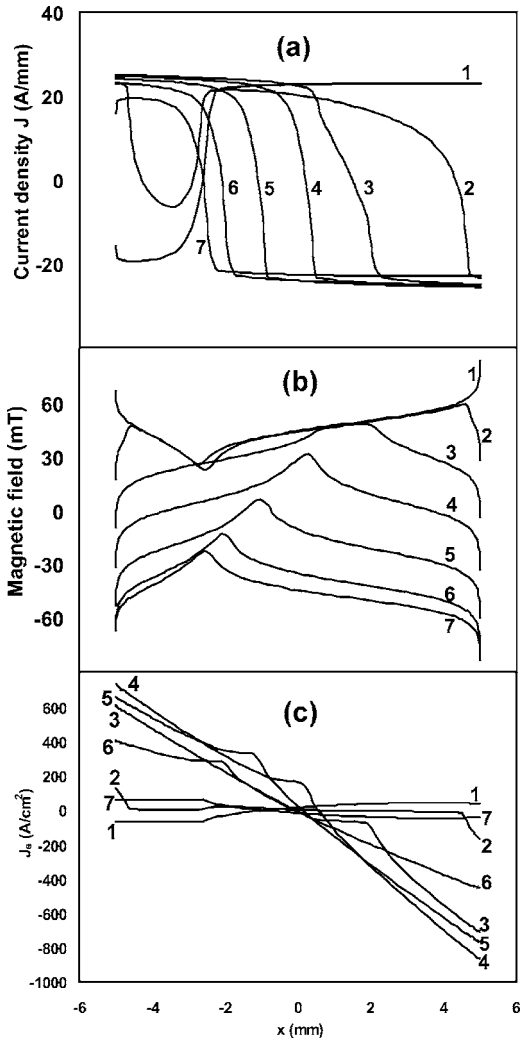

FIG. 10. Numerical results of (a) current density $J(y)$, (b) magnetic field $B(y)$, and (c) eddy current density $J_e(y)$ are plotted for the seven times indicated in Fig. 4.

In this case, Q_e is small in comparison with Q_f and Q_t and therefore can be ignored at this frequency (51 Hz). In the low current region, Q_f dominates, while Q_t becomes more significant when transport current is greater than 80 A. With the significant contribution of ferromagnetic loss, the transport loss calculated by Norris's model for the HTS layer is far below the measured transport loss. In Fig. 9, the numerical and experimental results of the total transport loss Q_{tt} are also plotted and good agreement is observed, especially at high current. The shielding effect of the ferromagnetic substrate might be small in this case since the loss is generated by self-field, not by an external magnetic field as in the previous case.

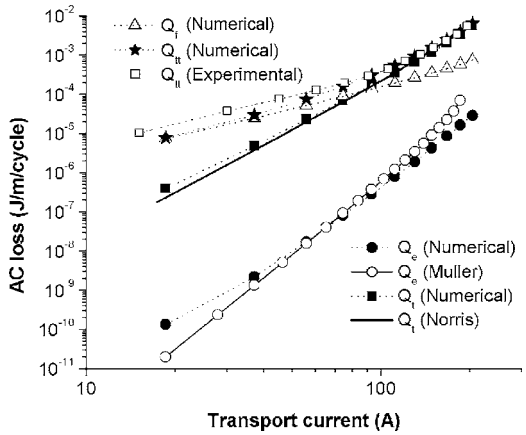

FIG. 9. Numerical results (dotted lines) of transport loss Q_t, ferromagnetic loss Q_f, eddy current loss Q_e, and total transport losses Q_{tt} at 51 Hz. Corresponding analytical results for Q_t and Q_e (solid lines) and experimental data (open square symbols) for Q_{tt} are also plotted.

C. Current carrying conductor in a perpendicular applied magnetic field

Lastly consider the case when the transport current and magnetic field simultaneously decrease from $I_0=130.2$ A ($I_0/I_c=0.7$), $H_0=50$ mT to $-I_0=-130.2$ A, $-H_0=-50$ mT. Figure 10 shows the distributions $J(y)$, $B(y)$, and $J_e(y)$ for the seven times shown in Fig. 4. These distributions show no symmetry whatsoever, so the calculations must be performed over the entire conductor width.

The ac loss generated in the HTS layer, Q_s, calculated numerically (open symbols) and analytically (solid lines) us-

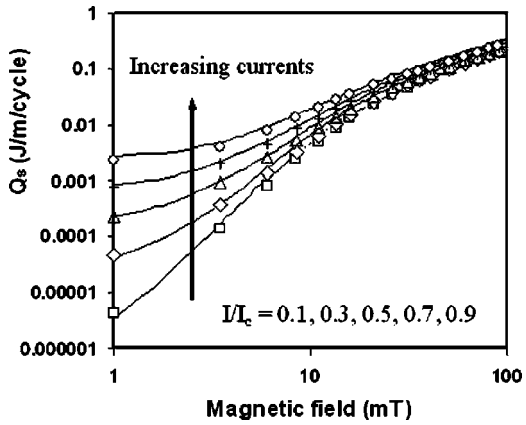

FIG. 11. The total loss Q_s is plotted for I/I_c=0.1, 0.3, 0.5, 0.7, and 0.9. Numerical (open symbols) and analytical results (solid lines) are seen.

ing Schönborg's equations[14] is plotted in Fig. 11. The numerical results reproduce the analytical results well. A slight variation between the two calculations in high-field and high current regions may be explained by the difference in the n value used in each calculation. In the numerical model, n =22, while in the analytical calculation, n is assumed to be infinite (critical state model).

Figure 12 shows that the total ac losses Q_{tt} obtained from numerical calculations (solid lines) are somewhat higher than those obtained experimentally (symbols) for transport currents I/I_c=0.1, 0.5, and 0.9 in applied field ranging from 1 to 100 mT. Good agreement between measured and calculated results for transport loss Q_t is seen in Fig. 13. Thus the differences between experimental and numerical results for Q_{tt} mainly result from the magnetization calculation.

All ac loss components, Q_m, Q_t, Q_f, and Q_e, are plotted in Fig. 14 for low transport current (I/I_c=0.1) and in Fig. 15 for high transport current (I/I_c=0.9) at a frequency of 51 Hz. For low transport current, the dominant source of loss is Q_m. Q_e is small and can be ignored in the low magnetic field region but increases quickly with magnetic field and becomes greater than Q_t and Q_f when $B_0>30$ mT. Q_e is important in the high-field region, especially with increasing frequency. For the high current case, Q_t is comparable to Q_m.

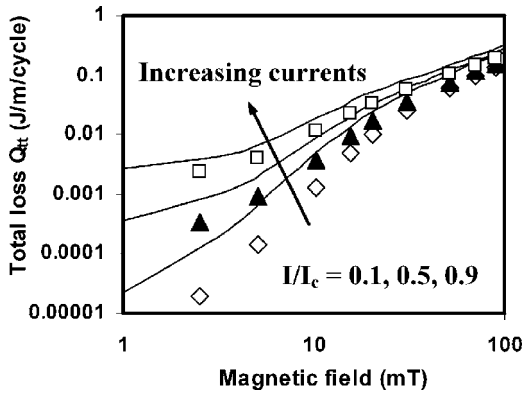

FIG. 12. The total ac loss Q_{tt} is plotted for I/I_c=0.1, 0.5, and 0.9. Numerical (solid lines) and experimental results (symbols) are seen.

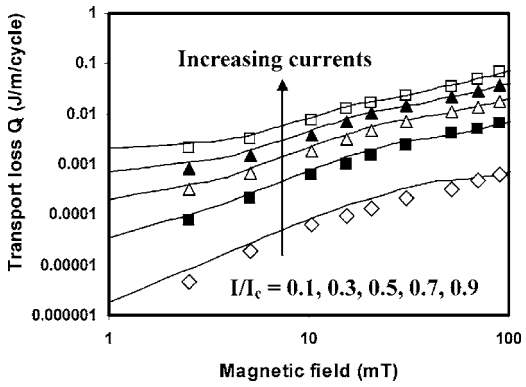

FIG. 13. Transport loss Q_t vs applied magnetic field for I/I_c=0.1–0.9 at 51 Hz. Numerical (solid lines) and experimental (symbols) results are shown.

Comparing Figs. 14 and 15, the change in transport current primarily affects Q_m, Q_f, and Q_e in the low magnetic field region ($B<10$ mT).

IV. SUMMARY

In this paper, a comprehensive numerical model is presented to calculate the total ac loss of YBCO coated conductors with a ferromagnetic substrate and Cu stabilizer. With the help of variable substitutions, the time varying current and magnetic field distributions for a superconducting strip are calculated. Comparing with analytical models in Refs. 9, 11, 12, and 14 the numerical model is successfully demonstrated to calculate all the individual loss components generated in the HTS layer, ferromagnetic substrate, and stabilizer. This is a key for understanding the contributions of each loss component to the total losses.

In this paper, the losses are calculated numerically for a variety of situations. Overall, Q_m and Q_t in the HTS layer are the dominant contributions to the total loss. The ferromagnetic losses are significant when there is transport current in zero background field, especially at low transport current. At a frequency of 51 Hz, the eddy current losses are considerable only at rather high values of applied field. Q_e increases rather rapidly with frequency and studies of Q_e at higher frequencies are needed. In this case, the numerical method becomes an effective tool since it is difficult to create experimentally a high field at high frequency, for instance, at 1 kHz.

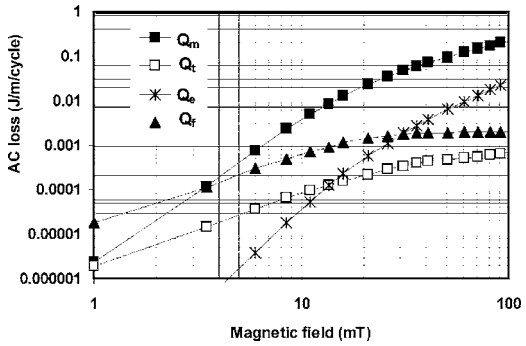

FIG. 14. Magnetization loss Q_m, transport loss Q_t, ferromagnetic loss Q_f, and eddy current loss Q_e vs applied magnetic field for I/I_c=0.1 at 51 Hz.

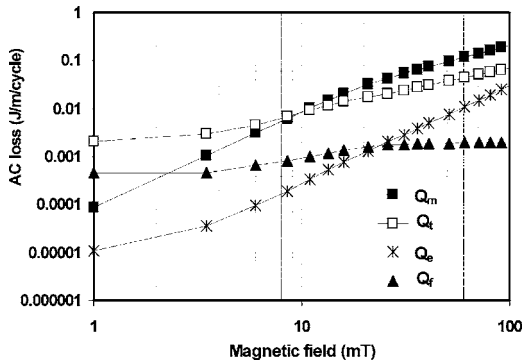

FIG. 15. Magnetization loss Q_m, transport loss Q_t, ferromagnetic loss Q_f, and eddy current loss Q_e vs applied magnetic field for $I/I_c=0.9$ at 51 Hz.

The presented model can be applied to the general case of simultaneous transport current and applied field with any phase difference between them. The differences between numerical and experimental results of magnetization loss can be improved easily by taking into account the actual properties of YBCO tapes, such as the relations $J_c(B)$, $n(B)$, and $J_c(y)$, which can be obtained experimentally. The shielding effect of a thick ferromagnetic substrate is another potential source of error in the magnetization loss calculations, but the problem becomes significantly more complicated when this effect is considered.

ACKNOWLEDGMENTS

This work was supported by DOE through the Center for Advanced Power Systems, Florida State University. The authors would like to thank Dr. Alexander Gurevich for his useful discussions.

[1]Y. Shiohara, Y. Kitoh, and T. Izumi, Physica C **445–448**, 496 (2006).
[2]V. Selvamanickam *et al.*, Proceedings of the Applied Superconductivity Conference, Seattle, WA, 28 August–1 September 2006 (unpublished).
[3]M. P. Oomen, J. Rieger, V. Hussennether, and M. Leghissa, Supercond. Sci. Technol. **17**, S394 (2004).
[4]D. Larbalestier, A. Gurevich, D. M. Feldmann, and A. Polyanskii, Nature (London) **414**, 368 (2001).
[5]M. D. Sumption, E. W. Collings, and P. N. Barnes Supercond. Sci. Technol. **18**, 122 (2005).
[6]D. T. Verebelyi *et al.*, Supercond. Sci. Technol. **16**, L19 (2003).
[7]Y. L. Xu and D. Shi, Tsinghua Science and Technology **8**, 342 (2003).
[8]K. Kakimoto, Y. Iijima, and T. Saitoh, Physica C **392–396**, 783 (2003).
[9]W. T. Norris, J. Phys. D **3**, 489 (1970).
[10]C. P. Bean, Phys. Rev. Lett. **8**, 250 (1962).
[11]K. H. Müller, Physica C **281**, 1 (1997).
[12]E. H. Brandt and M. Indenbom, Phys. Rev. B **48**, 12893 (1993).
[13]E. Zeldov, J. R. Clem, M. McElfresh, and M. Darwin, Phys. Rev. B **49**, 9802 (1994).
[14]N. Schönborg, J. Appl. Phys. **90**, 2930 (2001).
[15]J. Rhyner, Physica C **212**, 292 (1993).
[16]E. H. Brandt, Phys. Rev. B **54**, 4246 (1996).
[17]T. Yazawa, J. J. Rabbers, B. ten Haken, and H. H. J. ten Kate, J. Appl. Phys. **48**, 5652 (1998).
[18]D. N. Nguyen, P. V. P. S. S. Sastry, D. C. Knoll, G. Zhang, and J. Schwartz, J. Appl. Phys. **98**, 073902 (2005).
[19]E. H. Brandt, Phys. Rev. B **49**, 9024 (1993).
[20]E. H. Brandt, Phys. Rev. B **50**, 4034 (1994).
[21]O. Tsukamoto, H. Nakayama, S. Odaka, M. Ciszek, S. Hahakura, M. Ueyama, K. Ohmatsu, and D. Miyagi, Physica C **426–431**, 1290 (2005).
[22]D. N. Nguyen, P. V. P. S. S. Sastry, D. C. Knoll, and J. Schwartz, Supercond. Sci. Technol. **19**, 1 (2006).
[23]R. C. Duckworth, M. J. Gouge, J. W. Lue, C. Thieme, and D. T. Verebelyi, IEEE Trans. Appl. Supercond. **15**, 1583 (2005).
[24]A. O. Ijaduola, J. R. Thomson, A. Goyal, C. Thieme, and K. Marken, Physica C **403**, 163 (2004).
[25]G. Bertotti, *Hysteresis in Magnetism*, (Academic, San Diego, 1998).